

FULL PAPER

Open Access



# Evaluation of a method to derive ionospheric conductivities using two auroral emissions (428 and 630 nm) measured with a photometer at Tromsø (69.6°N)

Kazuhiro Adachi<sup>1</sup>, Satonori Nozawa<sup>1\*</sup> , Yasunobu Ogawa<sup>2</sup>, Asgeir Brekke<sup>3</sup>, Chris Hall<sup>4</sup> and Ryoichi Fujii<sup>1</sup>

## Abstract

This paper mainly aims at evaluating capabilities of derivation of ionospheric conductivities using two principal auroral emissions (427.8 and 630 nm). We have evaluated a photometric method of derivation of ionospheric conductivities based on simultaneous observations of a photometer (field of view =  $\sim 1.2^\circ$ ), a digital camera, and the EISCAT UHF radar (field of view =  $\sim 0.7^\circ$ ) operated at Tromsø, Norway (69.6°N, 19.2°E), for two nights on October 10 and 11, 2002. We have compared height-integrated Pedersen and Hall conductivities with a post-integration time of 10 s derived from EISCAT UHF radar observations and photometer observations with wavelengths of 427.8 and 630.0 nm. Sky images taken with the digital camera are utilized for distinguishing types of auroras in the views of the EISCAT UHF radar and the photometer. In general, a good agreement of temporal variations of the height-integrated Pedersen and Hall conductivities was found between EISCAT and photometer values. In cases of auroral arcs passing by in the field of view, however, differences in derived values between the two methods were found. Possible causes of the differences are discussed. We conclude that (1) the photometric method using 427.8 and 630 nm can capture temporal variations of the conductivities well, but unavoidable underestimations of the Pedersen (about 30–40%) and the Hall (about 50–60%) conductivities are involved, and (2) care is necessary for using photometric observational data when auroral arcs appear in the field of view.

**Keywords:** Auroral emission, Conductivity, Polar ionosphere, Photometer, EISCAT, Tromsø

## Introduction

The ionized component in the polar upper atmosphere (i.e., ionosphere) couples with both the magnetosphere and the thermosphere/mesosphere. One of the manifestations of the polar upper atmosphere is the three-dimensional (3D) current system: The magnetospheric currents, which occasionally flow along the earth's magnetic field lines into (or out of) the ionosphere, are connected to ionospheric currents in the ionospheric conducting layer (i.e., *E* region); consequently, the thermosphere is heated by Joule heating. Furthermore, thermospheric wind is

affected by ion motion through collisions between ions and neutrals (i.e., ion drag). Modeling of the physical interaction between the magnetosphere, ionosphere, and thermosphere therefore requires reliable realistic spatial and temporal distributions of the electric field, the energy of particle precipitation, and ionospheric conductivities. In particular, it is of vital importance to obtain the electrical properties of the ionosphere characterized by the Hall and Pedersen conductivities, because they affect the 3D current system, Joule heating, and so on.

Spatial and temporal distributions of the ionospheric electric field in the polar ionosphere can be obtained by using coherent radar systems (SuperDARN) (e.g., Greenwald et al. 1995). SuperDARN radars can provide the ionospheric electric field with temporal and spatial resolutions of about 2 min and about 45 km (down to

\*Correspondence: nozawa@nagoya-u.jp

<sup>1</sup> Institute for Space-Earth Environmental Research, Nagoya University, Furo-cho, Chikusa-ku, Nagoya, Japan

Full list of author information is available at the end of the article

15 km) over the polar ionosphere, respectively. On the other hand, it is generally difficult to obtain observationally spatial and temporal distributions of the ionospheric conductivities. The European Incoherent Scatter (EISCAT) UHF radar (Folkestad et al. 1983; Rishbeth and van Eyken 1993) can make height-resolved estimates of the ionospheric (Hall and Pedersen) conductivities and the ionospheric currents that were first derived from incoherent scatter (IS) radar measurements by the Chatanika IS radar (Brekke et al. 1974). Such studies have been carried through by measurements obtained by the EISCAT UHF radar (e.g., Brekke and Hall 1988; Fontaine and Peymirat 1996; Sugino et al. 2002a, b). However, IS radar measurements are usually limited in space and time. Imagers onboard satellites can provide ionospheric physical parameters with a good spatial coverage. A suitable multi-wavelength observation of auroral emissions allows one to derive the energy distribution of the auroral particles (see a review by Robinson and Vondrak 1994). The global auroral conductance distribution has been estimated with auroral imagers onboard satellites (e.g., Coumans et al. 2004). The spatial resolution of the auroral imagers on satellites is typically about a hundred kilometers and is insufficient for determining the distribution of the ionospheric currents, because the spatial scale of a large-scale field-aligned current (FAC) covers a few hundred kilometers or less. Measurements with several tens of kilometers of spatial resolution of the ionospheric conductivity are needed to determine the FAC distribution from the spatial gradient of the ionospheric currents.

On the other hand, if ground-based optical observations are made at multiple stations, they are capable of providing spatial and temporal distributions of auroras with a high spatial and temporal resolution, although successful observations require a dark clear sky. Nocturnal ionospheric conductance can be inferred from optical data sets. There are several combinations of auroral wavelengths to infer characteristic energies and energy fluxes of the precipitating auroral electrons (e.g., Lanchester et al. 2009). Among them, the emission intensities at wavelengths of 427.8 nm ( $N_2^+$  first negative band) and 630.0 nm [metastable atomic state  $O(^1D)$ ] can be used to infer the characteristic energies and energy fluxes of them (Niciejewski et al. 1989; Rees and Luckey 1974). The emission intensity at 427.8 nm is related directly to the energy flux, and the intensity ratio of 427.8 to 630.0 nm is related to the characteristic energy (e.g., Vondrak and Sears 1978).

Some comparative studies of the ionospheric conductance derived with an optical instrument and an IS radar have been conducted. Mende et al. (1984) compared conductances (i.e., height-integrated conductivities) derived from auroral spectroscopic measurements with

those from the Chatanika IS radar (64.9° geomagnetic north). Although, in general, fairly good agreement was found between values derived by these different methods, disagreements between them indicate limitations of each experimental technique. Mende et al. (1984) summarized that the IS radar yielded more accurate values of the conductance with a limited temporal and spatial resolution, while the optical measurements provided less accurate values with higher temporal resolution and wider spatial region. Robinson et al. (1989) confirmed qualitatively the empirical relationship between the auroral luminosities observed with an auroral imager onboard the Dynamics Explorer 1 (DE 1) satellite and the Hall and Pedersen conductance derived from the Chatanika IS radar. Vondrak et al. (1985) used simultaneous and common-volume observations from the auroral scanning photometer onboard ISIS 2 and from the Chatanika IS radar and showed that ionospheric electron density profiles were determined from the emissions of  $N_2^+$  and neutral atomic oxygen at 391.4 and 630.0 nm. Robinson et al. (1992) compared electron density measurements from the Søndre Strømfjord (67°N, 51°W) IS radar with electron densities inferred from OI (135.6 nm) and  $N_2^+$  (391.4 nm) emissions observed by the auroral ionospheric remote sensor (AIRS) onboard the Polar Bear satellite and found a good agreement between the measured and inferred profiles. These studies show that the multi-wavelength optical method has an ability to provide ionospheric conductivities. However, the methods have not yet been well evaluated qualitatively in detail.

To evaluate a multi-wavelength optical method for derivation of ionospheric conductivities in more detail, simultaneous observations are needed that last for several hours or longer with optical instruments and an IS radar. Lanchester et al. (2009) have estimated average energy and flux of precipitation electrons using simultaneous images of aurora and EISCAT radar data obtained at Tromsø (geographic coordinates of 69.6°N, 19.2°E) and found a relatively good agreement between electron density modeled by the  $N_2$  1P band emissions (670 nm) and density profiles measured directly with the EISCAT UHF radar with a time resolution of 0.44 s. Peak electron densities derived from the two methods, however, were sometimes different, and density profiles observed with the EISCAT UHF radar showed large fluctuations in a height range above 120 km (see Fig. 7 in Lanchester et al. 2009). The differences and fluctuations would cause uncertainty of the Hall and Pedersen conductivities. Ion recombination time constant would also cause an uncertainty when the average energy and flux of precipitation electrons are calculated from electron density profiles. The time constant under electron density of a few  $10^{11} \text{ m}^{-3}$  is about 10 s (see Fig. 3 in Semeter and Kamalabadi 2005).

To validate a multi-wavelength method for derivation of ionospheric conductivities qualitatively, we conducted photometric observations continuously during darkness intervals from October 2002 to March 2003 at the EISCAT Tromsø site in Norway. The photometer was pointed toward the local magnetic field-aligned direction at the Tromsø EISCAT site. In this paper, we aim at evaluating the method for derivation of conductivities by photometer using two wavelengths (427.8 and 630 nm). We present a comparison of ionospheric conductivities derived from the EISCAT UHF radar and the four-wavelength photometer for two nights on October 10 and 11, 2002. It should be pointed out that although usage of 844.6 nm emission would be better (cf. Ono 1993), this paper aims at evaluation and presenting capabilities of the usage of the two emission lines (427.8 and 630.0 nm). This is because the two lines are principal auroral emissions as well as easy to use, and few evaluation studies have been conducted.

## Methods

The electron density data analyzed in this study were obtained with the tristatic EISCAT UHF radar, the so-called Kiruna–Sodankylä–Tromsø (KST) UHF radar system whose field of view is  $\sim 0.7^\circ$ . We analyzed Common Program One (CP1) mode (Collis 1995) data. In the CP1 mode, the transmitting antenna at Tromsø is fixed along the local geomagnetic field direction. The physical parameters directly measured are electron density, electron/ion temperatures, and ion drift velocity. Electron density profiles were calibrated by ionosonde (Hall and Hansen 2003) data obtained simultaneously at the same observational field. Post-integration of the EISCAT radar data is made to reduce the noise level, and EISCAT data with post-integrated time of 10 s were used in this study.

Optical data used in this study were obtained with a four-wavelength photometer and a digital camera collocated with the EISCAT UHF radar at Tromsø. The four-wavelength photometer has a field of view of about  $1.2^\circ$  and was pointed along the local magnetic field line as well; the EISCAT radar and the photometer conducted common-volume measurements. Auroral lights with different wavelengths were fed into four channels by beam splitters and dichroic mirrors. The photometer has two dichroic mirrors used for separating blue and infrared wavelengths. Interference filters at 427.8, 630.0, 670.5, and 844.6 nm were selected based on Ono (1993) to obtain characteristic auroral emissions. Auroral emissions after the interference filters were detected by four photo-multipliers. Two wavelengths of emissions at 427.8 and 630.0 nm were utilized in this paper. Intensity of the photometer was calibrated by a calibration system at the

National Institute of Polar Research (NIPR) in Japan. The transmission curves of the filters were measured by illuminating a diffuse screen with a scanning grating monochromator at NIPR. The filter efficiency for 427.8 nm was obtained by integrating, in wavelength, the product of the normalized filter transmission curve and the normalized synthetic spectrum at 300 K calculated following Kurihara (2004). Photometer data were obtained with an A/D board, and their time resolution reached 0.1 s. Images of the digital camera were used for monitoring auroral structures as well as weather conditions. The field of view of the digital camera was about  $90^\circ \times 60^\circ$  (about  $240 \times 140$  km at 120 km height) with a fish-eye lens. We obtained sky images every minute with an exposure time of 8 s.

The Pedersen and Hall conductivities are calculated using the formulae by Brekke and Hall (1988) and the NRLMSISE-00 neutral atmospheric model (Picone et al. 2002). We derived the Pedersen and Hall conductivities ( $\sigma_P$  and  $\sigma_H$ , respectively, in S/m) from the following formulae:

$$\sigma_P = \frac{N_e e}{B} \left[ \frac{\omega_e \nu_{en}}{\omega_e^2 + \nu_{en}^2} + p_{i1} \frac{\omega_{i1} \nu_{i1n}}{\omega_{i1}^2 + \nu_{i1n}^2} + p_{i2} \frac{\omega_{i2} \nu_{i2n}}{\omega_{i2}^2 + \nu_{i2n}^2} \right] \quad (1)$$

$$\sigma_H = \frac{N_e e}{B} \left[ \frac{\omega_e^2}{\omega_e^2 + \nu_{en}^2} - p_{i1} \frac{\omega_{i1}^2}{\omega_{i1}^2 + \nu_{i1n}^2} - p_{i2} \frac{\omega_{i2}^2}{\omega_{i2}^2 + \nu_{i2n}^2} \right] \quad (2)$$

where  $e$  is the electron charge (in C),  $B$  is the magnitude of the earth's geomagnetic field (in T),  $N_e$  is the electron density (in  $\text{m}^{-3}$ ),  $\omega_i$  and  $\omega_e$  are the angular gyro frequencies (in Hz) of ions and electrons, respectively, and  $\nu_{en}$  and  $\nu_{in}$  are collision frequencies (in Hz) between ions or electrons and neutral species, respectively. Here plasma neutrality and two different single charged ion species are assumed with the relative parameter contributions  $p_{i1}$  and  $p_{i2}$ . The geomagnetic field  $B$  is calculated from the International Geomagnetic Reference Field model (IGRF-2000) (Olsen et al. 2000) for the appropriate geographic position. The two ion species are assumed to have ion masses  $m_{i1} = 30.5$  and  $m_{i2} = 16$  amu. The lighter ion is assumed to be atomic oxygen, and the heavier ion species are assumed to consist of  $\text{NO}^+$  (75%) and  $\text{O}_2^+$  (25%). The relative abundance of the lighter ( $\text{O}^+$ ) and the heavier ion ( $\text{NO}^+$ ,  $\text{O}_2^+$  mixture) is given by the International Reference Ionosphere (IRI) (Bilitza 2001). For the electron neutral collision frequency ( $\nu_{en}$ ) and the ion neutral collision frequencies ( $\nu_{i1n}$  and  $\nu_{i2n}$ ), we use the following formula:

$$\begin{aligned} \nu_{en} = & 2.33 \times 10^{-17} \times n(\text{N}_2) \times (1 - 1.21 \times 10^{-4} \times T_e) \\ & \times T_e + 1.82 \times 10^{-16} \times n(\text{O}_2) \\ & \times (1 + 3.6 \times 10^{-2} \times \sqrt{T_e}) \times \sqrt{T_e} + 8.9 \\ & \times 10^{-17} \times n(\text{O}) \times (1 + 5.7 \times 10^{-4} \times T_e) \times \sqrt{T_e} \end{aligned} \quad (3)$$

$$\nu_{in} = [4.29 \times n(\text{N}_2) + 4.23 \times n(\text{O}_2) + 2.41 \times n(\text{O})] \times 10^{-16} \quad (4)$$

$$\begin{aligned} \nu_{2n} = & 6.82 \times 10^{-16} \times n(\text{N}_2) + 6.66 \times 10^{-16} \times n(\text{O}_2) \\ & + 3.42 \times 10^{-17} \times n(\text{O}) \times \sqrt{T_r} \\ & \times (1.08 - 0.139 \times \log_{10} T_r + 4.51 \times 10^{-3} \times (\log_{10} T_r)^2) \end{aligned} \quad (5)$$

where  $n(\text{N}_2)$ ,  $n(\text{O}_2)$ , and  $n(\text{O})$  are densities of  $\text{N}_2$ ,  $\text{O}_2$ , and  $\text{O}$  (in  $\text{m}^{-3}$ ),  $T_n$ ,  $T_e$ , and  $T_i$  are the neutral, electron, and ion temperatures (in K), respectively,  $T_r = (T_i + T_n)/2$ . These formulae are given by Schunk and Nagy (1978) for the electron neutral collision frequency and by Schunk and Walker (1973) for the ion neutral collision frequencies. The height-integrated Pedersen and Hall conductivities ( $\Sigma_p$  and  $\Sigma_H$ , respectively, in  $S$ ) can be obtained from the following formulae:

$$\Sigma_p = \int_{z_1}^{z_2} \sigma_p dz \quad (6)$$

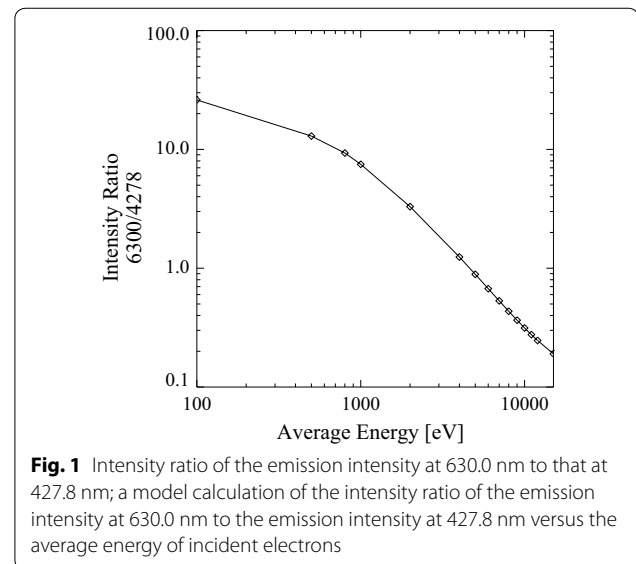
$$\Sigma_H = \int_{z_1}^{z_2} \sigma_H dz \quad (7)$$

where  $z_1$  and  $z_2$  are set to be 90 and 180 km, respectively. We used the NRLMSISE-00 model for the neutral temperature and densities. Although the EISCAT radar can provide electron and ion temperature values, we used the IRI model predictions. This is because here we use data with a 10-s temporal resolution that is too short for the EISCAT radar to provide the temperature values properly. It should be noted that we had compared conductivity values derived by using the temperatures from the IRI predictions and the EISCAT data with a 1-min resolution and found that there is good agreement (the difference being less than 1%, not shown here).

In order to derive the average energy and the energy flux from auroral emission intensities, we utilized the results of the model calculation in Ono (1993), except for the energy distribution of incident electrons and the atmospheric model. We first derived separately the primary and secondary electron spectra by solving an electron transport equation that was approximated on the basis of the two-stream method (cf. Solomon et al. 1988; Banks and Nagy 1970; Nagy and Banks 1970). Based on the calculated intensity spectra of auroral electrons,

volume emission rates were obtained for 427.8 and 630.0 nm taking into account physical and chemical processes (see Table 2 in Ono 1993). In this study, contrary to Ono (1993) who used a Gaussian type, the incident auroral electron fluxes were modeled by the Maxwellian energy distribution with an average energy and an energy flux (see Eq. 8). The validity of assuming the Maxwellian energy distribution will be addressed in the discussion session. Figure 1 shows a result of the model calculation for determining average energies of incident electrons based on the measured intensity ratio of 630.0 to 427.8 nm. The total energy flux was directly calculated using the measured intensity of 427.8 nm. The electron density profiles were calculated using the ionization rate that was derived from the average energy and flux of precipitating electrons based on the Ono (1993) model. The Pedersen and Hall conductivities can be calculated from Eqs. (1) and (2), respectively, using the electron density and collision and gyro frequencies.

It should be pointed out that we did not use low intensity data where the intensity of 630 nm emissions was lower than the criterion described below. This is because we cannot distinguish airglow (usually less than about 100 R) or town light from aurora light, and the ambiguities of such cases become significantly larger. The criterion value was determined as follows: (1) we calculated a mean value (called, “first mean value”) with a standard deviation using all the data sets throughout the night, (2) we calculated a mean value (“second mean value”) using data whose values are less than the first mean value plus the standard deviation, and (3) the second mean value is used as a background level value and consequently is used as a criterion value. For example, from 18:00 to



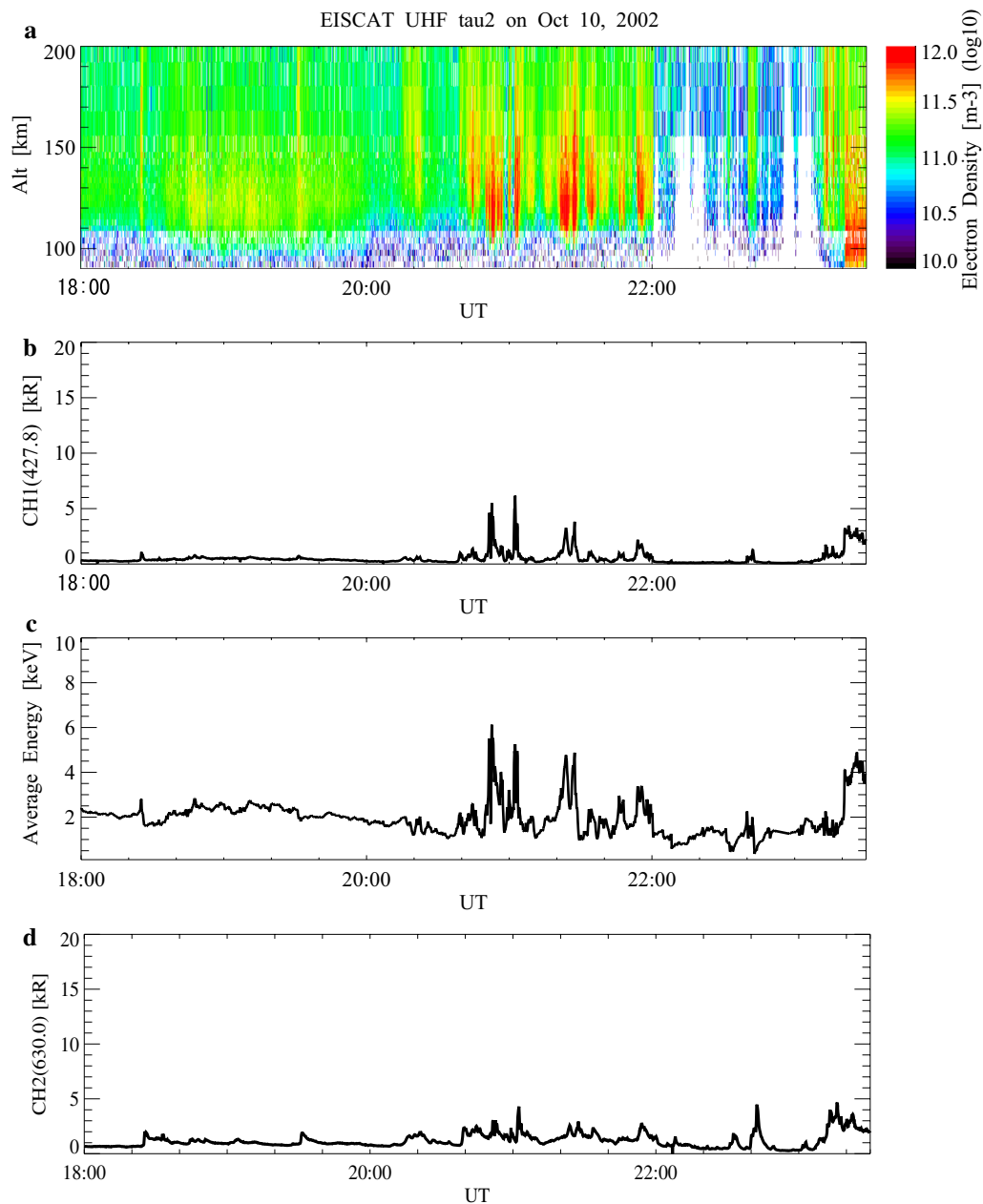


**Fig. 2** EISCAT and photometer results for October 10, 2002; **a** time–altitude profiles of electron density obtained with the EISCAT UHF radar from 18:00 UT to 23:30 UT on October 10, 2002. **b** Temporal variation of the emission intensity at 427.8 nm observed by the photometer. **c** Temporal variation of the average energy of the precipitating electrons derived from the emission intensity ratio of 427.8 to 630.0 nm from the photometer observations. **d** Temporal variation of the emission intensity at 630.0 nm observed by the photometer

23:30 UT on October 10, 2002, the criterion value was about 0.7 kR.

## Results

### Case of October 10, 2002

Figure 2a shows temporal and altitude variations of the electron density between 90 and 200 km observed with

the EISCAT UHF radar between 18:00 and 23:30 UT (UT = LT – 1 h) on October 10, 2002. Figure 2b, d shows a temporal variation of the emission intensity at 427.8 and 630.0 nm, respectively, observed with the photometer during the same interval. Figure 2c shows a temporal variation of the average energy of the precipitating electrons derived using two wavelength (427.8 and 630 nm)

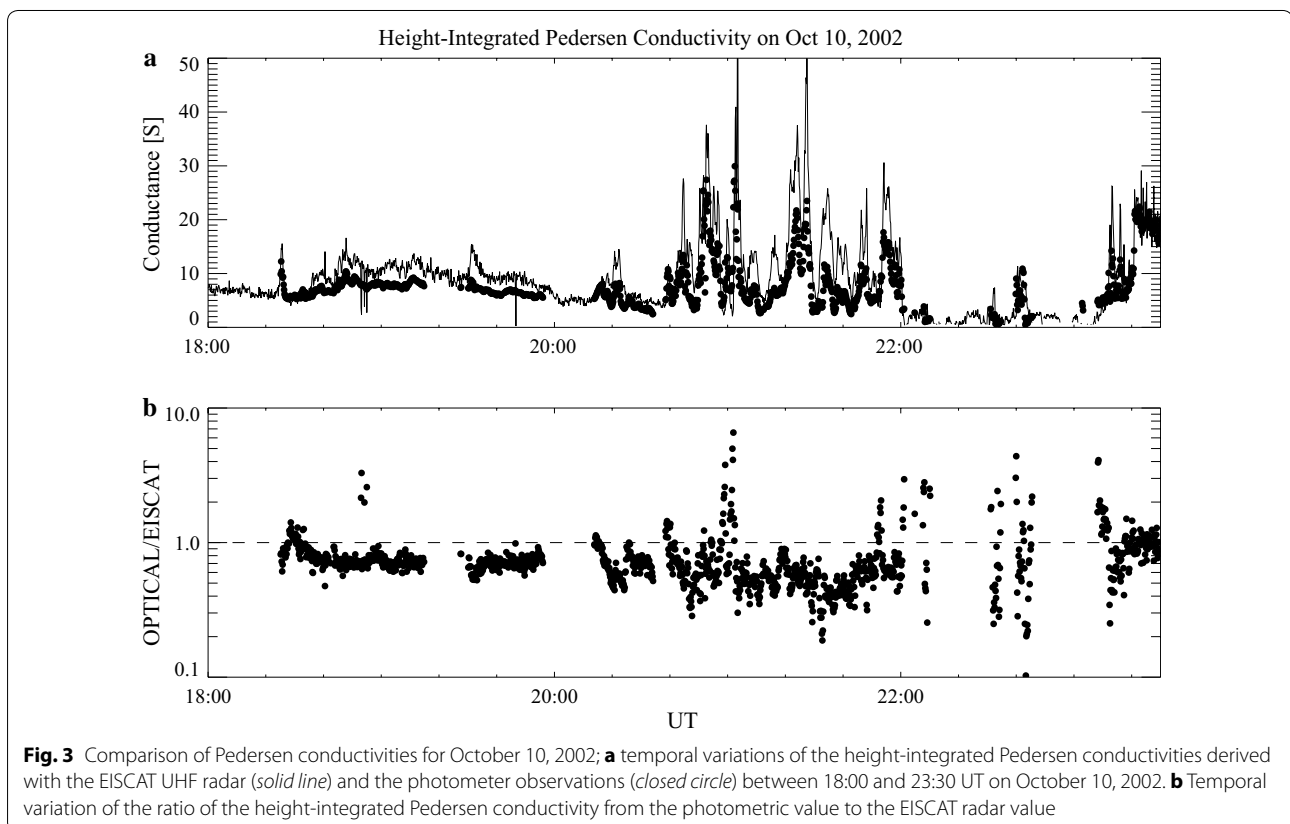


photometer measurements. The EISCAT observations show continual particle precipitation (sometimes intermittent strong particle precipitation) occurring between 18:00 and 22:00 UT, and strong particle precipitation between 23:20 and 23:30 UT following an interval with almost no electron precipitation interval between 22:00 and 23:10 UT. It should be noted the electron density in the *E* region rapidly (e-folding time being less than about 5 min) becomes lower due to dissociative recombination processes (Heinselman 2000). Thus, when no auroral particle precipitation occurs, such as the interval between about 22:00 and 23:10 UT, the electron density was very low. Observed enhancements of the emission intensity at 427.8 nm shown in Fig. 2b correspond well to the intermittent strong particle precipitations (i.e., enhancements of the electron density shown in red in Fig. 2a) and exceeded about 2 kR, while the temporal variation of 630.0 nm emission shows different features from that of 427.8 nm. The derived average energy shown in Fig. 2c varied with time and was about 1–2 keV for most of the time interval, but became about 4–6 keV when the electron density was enhanced below 110 km as seen in the EISCAT observations. Between 22:00 UT and 23:10 UT, the electron density below 150 km was very low and the emission intensity of 427.8 nm was lower than 1 kR for almost the entirety of the time interval, while that of

630.0 nm shows an enhancement up to about 4.5 kR at around 22:42 UT.

Figure 3a compares temporal variations of the height-integrated Pedersen conductivity derived with the EISCAT UHF radar (solid line) and the photometer (closed circles) observations between 18:00 and 23:30 UT on October 10, 2002. In general, the temporal variations of the conductivity derived from the two methods correspond well to each other, while there is a tendency for the conductivity values from the photometer observations to be lower than those derived from the EISCAT observations. This is confirmed in Fig. 3b, which shows ratios of Pedersen conductivities. The mean ratio of Pedersen conductivities derived by the photometric method to those by EISCAT is about 0.79, and the ratio is relatively constant with time except for some intervals. Around 18:52 UT, the electron density became lower, and the ratio increased. This is true for the other cases (around 20:59–21:03, around 2152, around 22:00 UT) when the ratio exceeded 1. The most probable reason would be the size difference of the fields of view: The photometer observed a wider area ( $\sim 1.2^\circ$ ) than that of the EISCAT measurements ( $\sim 0.7^\circ$ ).

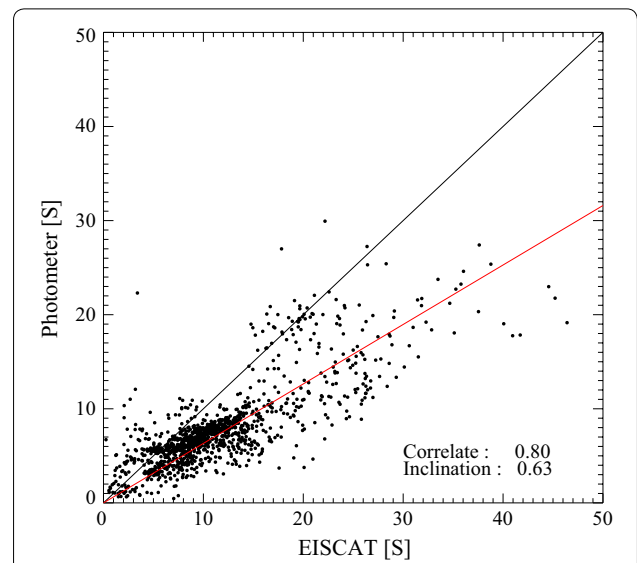
Between 23:20 and 23:30 UT, both the conductivity values are in good agreement and the ratio is scattered about 1. However, the derived average energy was about



4–5 keV as shown in Fig. 2c. In Fig. 2a, the EISCAT UHF radar captured high electron density below 100 km, indicating particle precipitation with the higher energy (>30 keV) occurred. In this case, our derived average energy would be wrong. We will back to this later in this chapter.

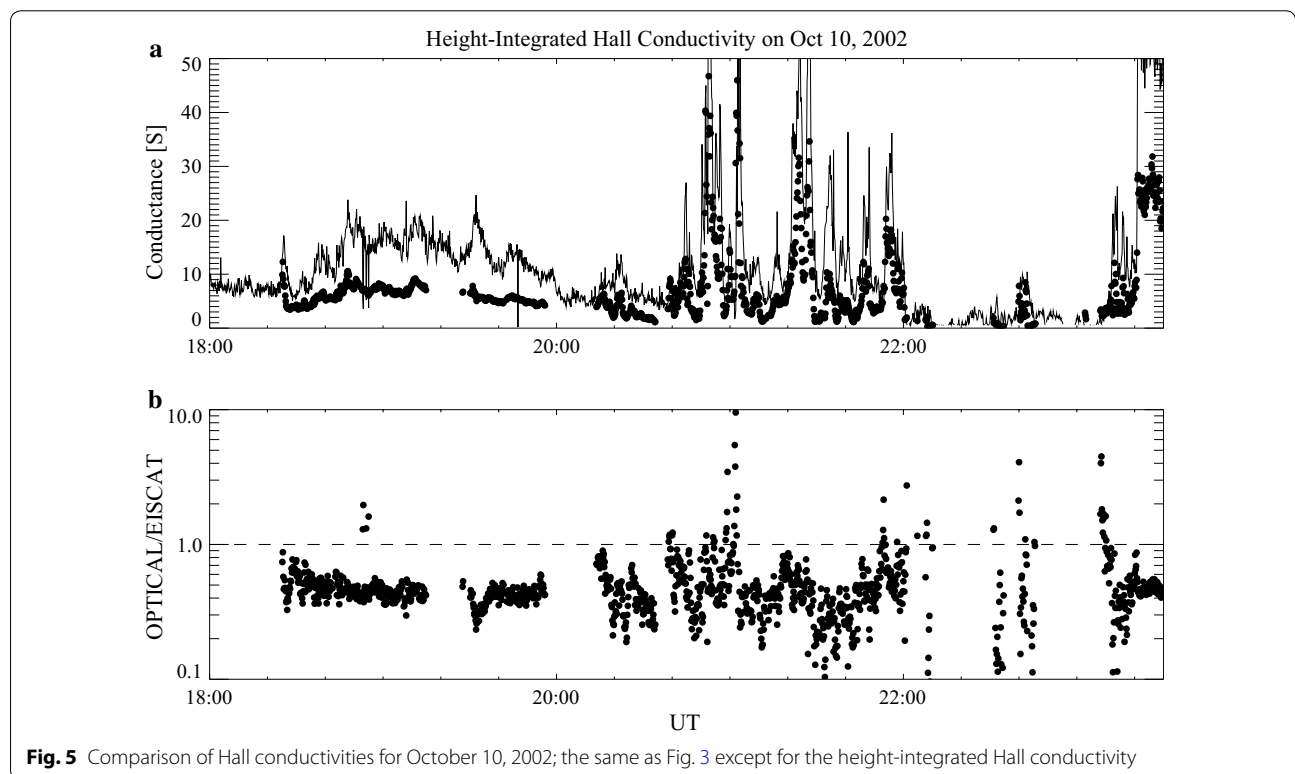
Figure 4 shows a scatter plot of the height-integrated Pedersen conductivity derived from the two methods. The cross-correlation coefficient is about 0.80, essentially indicating that the photometer method can capture the temporal variation well, while the conductivities tend to be underestimated with the photometer by about 40% since the inclination is about 0.6.

Figure 5a compares temporal variations of the height-integrated Hall conductivity from the two methods between 18:00 and 23:30 UT on October 10, 2002. Figures 5b and 6 show the ratio and a scatter plot of the height-integrated Hall conductivity values, respectively, for the same time interval. The temporal variations of the height-integrated Hall conductivity derived from the two methods again correspond well where the correlation coefficient between values from the two methods is about 0.86. The ratio exhibits a stable temporal variation for periods when the electron density observed by EISCAT became low. Similar to the cases of the Pedersen conductivity, in general, the values derived from the EISCAT radar are larger than those derived from the photometer.

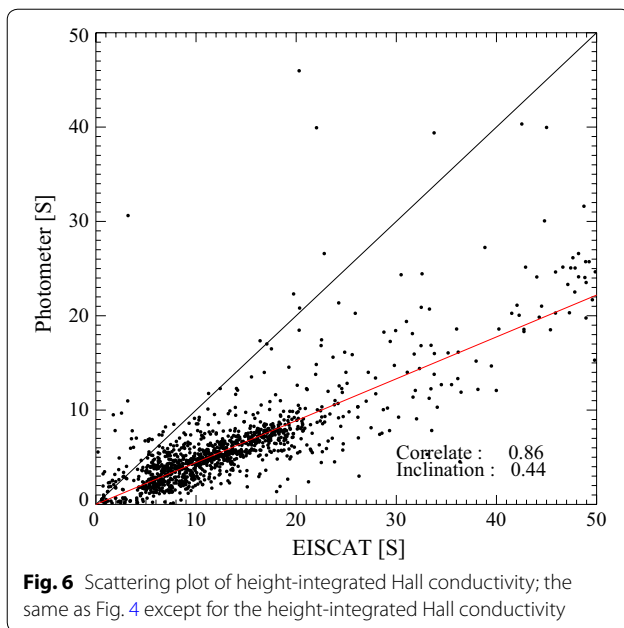


**Fig. 4** Scatter plot of height-integrated Pedersen conductivity for October 10, 2002; scatter plot of the height-integrated Pedersen conductivity derived with the EISCAT UHF radar (abscissa) and the photometer (ordinate) observations for the night of October 10, 2002

Between 23:20 and 23:30 UT, the ratio was about 0.5, and in the case of Pedersen conductivity the ratio was about 1. Because the atmosphere below 100 km was ionized, the peak energy of the precipitation electron would be about



**Fig. 5** Comparison of Hall conductivities for October 10, 2002; the same as Fig. 3 except for the height-integrated Hall conductivity



30 keV (cf. Rees 1963). This would suggest the limitation of the photometric method using 427.8 and 630 nm for the case of high-energy precipitation.

#### Case of October 11, 2002

Figure 7 shows (a) temporal and altitude variations of the electron density observed by EISCAT, (b) the emission intensity at 427.8 nm, (c) the derived average energy of the precipitating electrons, and (d) the emission intensity at 630.0 nm, over 8 h from 18:00 UT on October 11 to 02:00 UT on October 12, 2002. Figures 8a and 10a compare temporal variations of the height-integrated Pedersen and Hall conductivities, respectively, derived by the two methods for the same time interval. Figures 8b and 10b show the ratios of conductivities by photometer to those by EISCAT, and Figs. 9 and 11 present scatter plots of the height-integrated Pedersen and Hall conductivities, respectively. Relatively strong auroral particle precipitation (as shown in Fig. 7a, b) was captured with both the EISCAT radar and the photometer on several occasions during the interval. In particular, the electron density was enhanced below 110 km, suggesting occurrence of high-energy particle precipitation (cf. Rees 1973) on (at least) five occasions: around 20:25, around 20:40, and around 23:26 UT on October 11, and around 00:00 and around 00:40 UT on October 12. The strong precipitation lasted for a few tens of seconds to about 10 min. In the case of the strong particle precipitation occurring at around 20:25 UT on October 11, the emission intensity at 427.8 nm reached about 14 kR, and the corresponding average energy was about

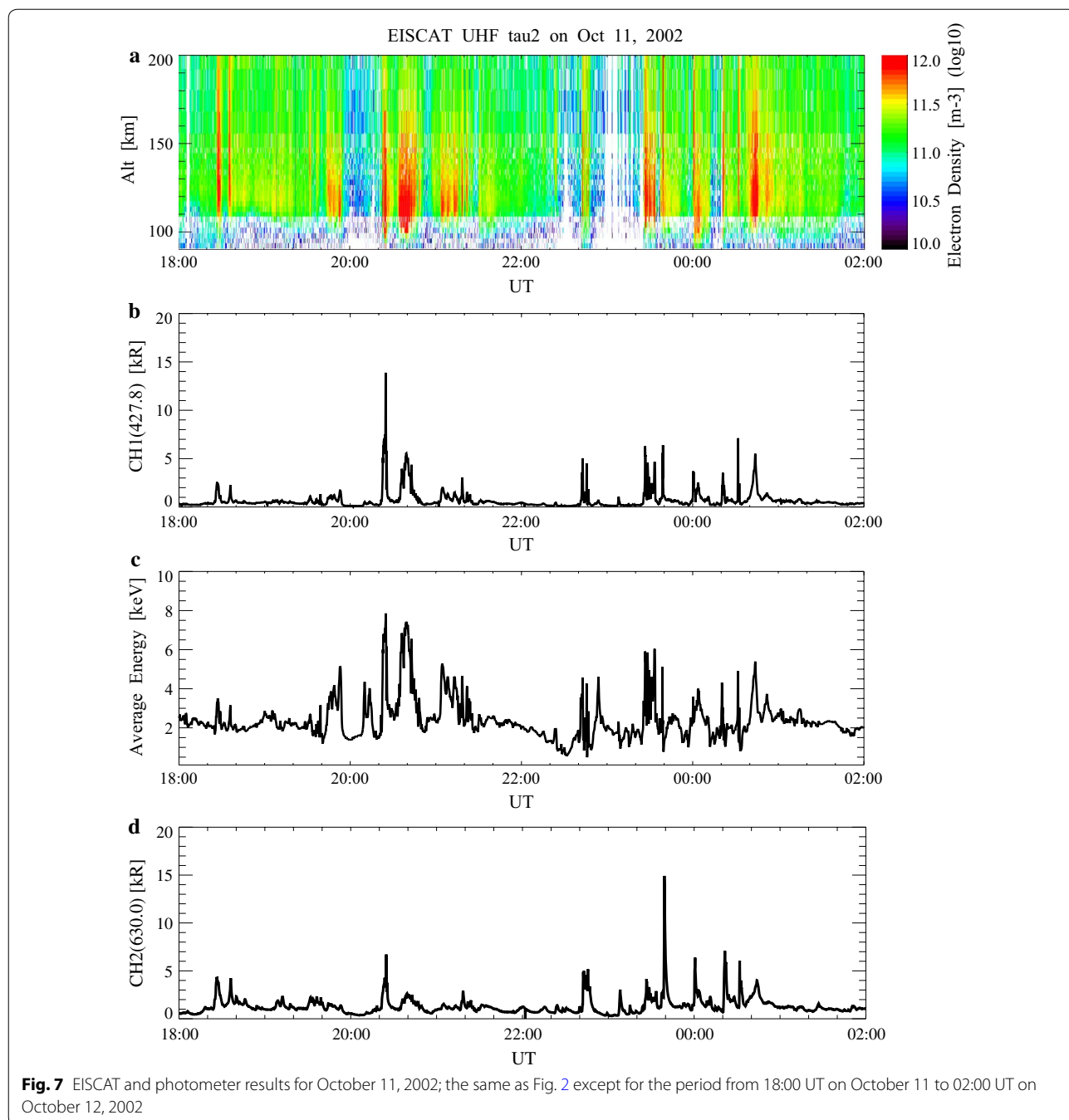
8 keV. It appears to be true that when the electron density was enhanced below 110 km, the emission intensity at 427.8 nm became larger ( $>5$  kR) and the average energy was also larger ( $>4$  keV). The ratios (as shown in Figs. 8b, 10b) of the conductivities reached about 3 (i.e., the conductivities derived from the photometer were larger than those derived from the EISCAT measurements) just after the peak intensity (at about 20:25 UT). For the other cases when the ratios became larger, the electron density from the EISCAT measurements denoted lower values, but the emission intensity at 427.8 nm was not much lower. These happened just before or after the enhancements of the electron density (EISCAT) and the emission intensity (427.8 nm), most probably the arc passed by the views of the EISCAT radar and the photometer. Except for these time intervals, the ratios (both Pedersen and Hall conductivities) were relatively constant (about 0.9 and 0.6, respectively). The temporal variations of the conductivities correspond well to each other, and their correlation coefficients are about 0.84 for the Pedersen conductivity and 0.86 for the Hall conductivity. These results suggest the photometric method worked reasonably well, but a non-negligible underestimation occurred by the photometric method.

At last, it should be pointed out that the temporal scattering of the ratios (as shown in Figs. 3b, 5b, 8b, 10b) is probably due to the different sizes of the views of the two instruments, and thus, the scattering does not indicate a problem in the photometric method.

#### Discussion

As presented in the previous session, the temporal variations of the conductivities derived from the two methods correspond well to each other, but the conductivity values from the photometer observations using 427.8 and 630.0 nm are generally lower than those derived from the EISCAT observations. In the case of the Pedersen conductivity, the inclinations of the linear fitting are about 0.6–0.7, while those of the Hall conductivity are 0.4–0.5, meaning that the Hall conductivity values from the photometer are almost half the values of those from EISCAT measurements. Here we discuss possible causes of the difference, such as (1) unsuitable assumption of the shape of the energy spectrum of the precipitating particles, (2) the long lifetime ( $\sim 110$  s) of the  $O(^1D)$  state (630 nm line), (3) contamination/scattering of the emission line due to the atmosphere, (4) possible contributions from proton precipitations, (5) collision cross section between atomic oxygen and electron, and (6) composition of the atmosphere predicted by NRLMSISE-00. Finally, we have also examined effects of the cross section and the atomic oxygen density.



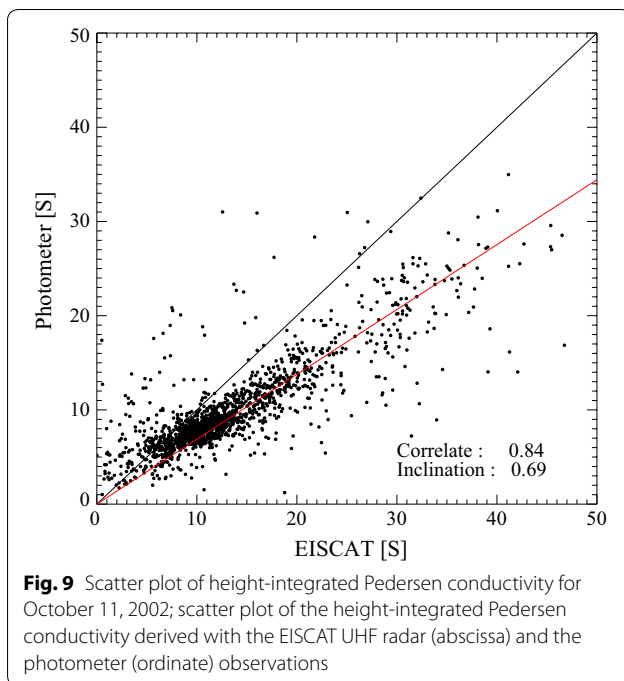
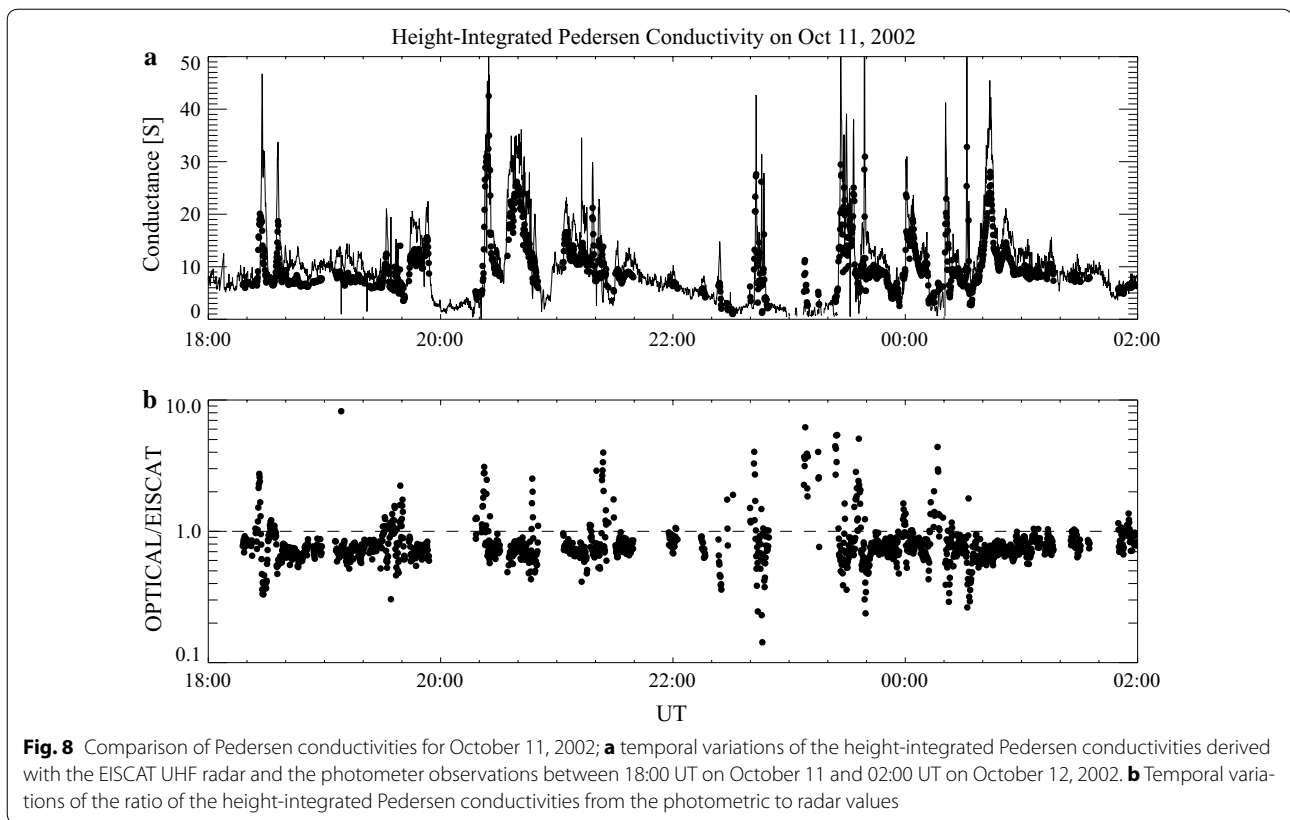


### Shape of the energy spectrum

The shape of the energy spectrum is assumed to be the Maxwellian distribution using a formula by Strickland et al. (1993). Incident differential electron number flux  $\phi_0(E)$  can be obtained as follows:

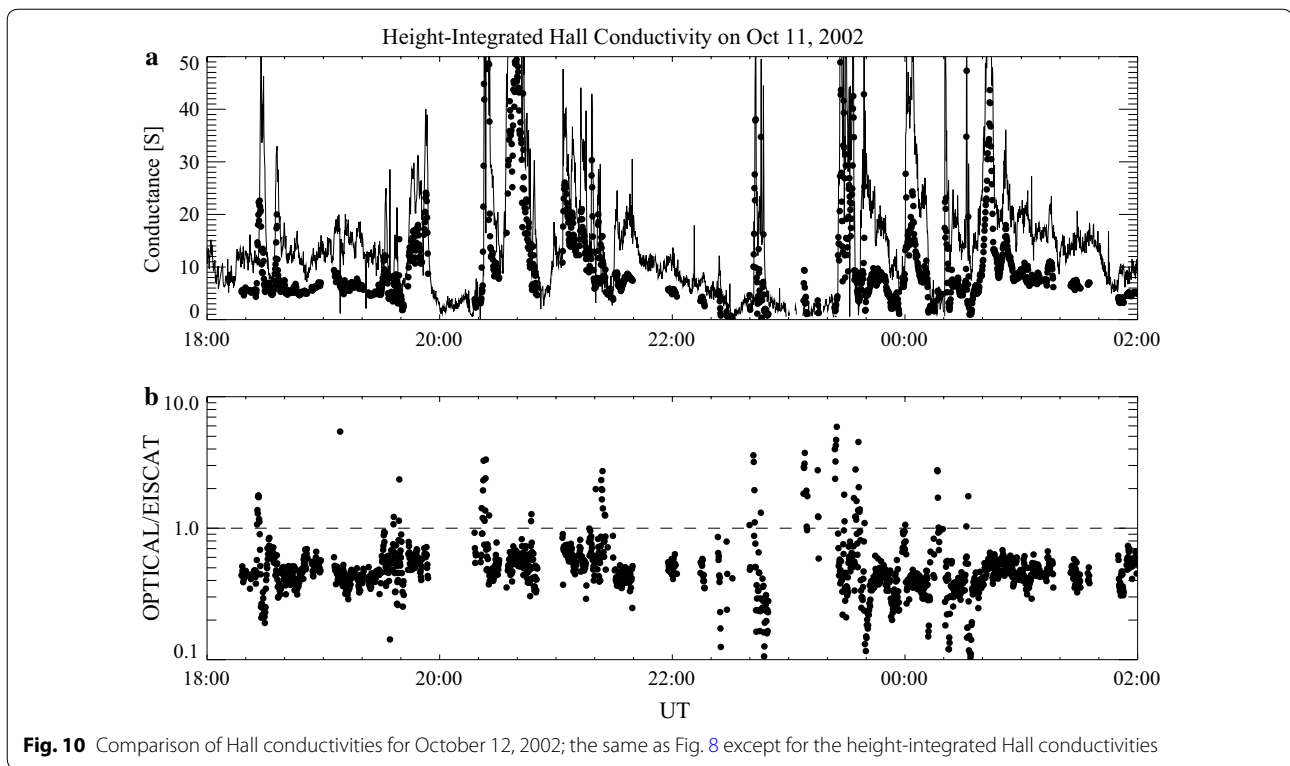
$$\phi_0(E) = \frac{Q_M}{2E_M^3} E \exp\left[\frac{-E}{E_M}\right] \quad (8)$$

where  $E$  is the energy of the electron,  $E_M$  the characteristic energy, and  $Q_M$  the energy flux. The Maxwellian distribution has been widely used in these kinds of studies since Rees and Luckey (1974) introduced it. It is believed that the Maxwellian distribution can be well applied to the energy spectra of the precipitating particles that cover a wide spatial region such as a diffuse aurora. It was shown by satellite observations, however, that the energy



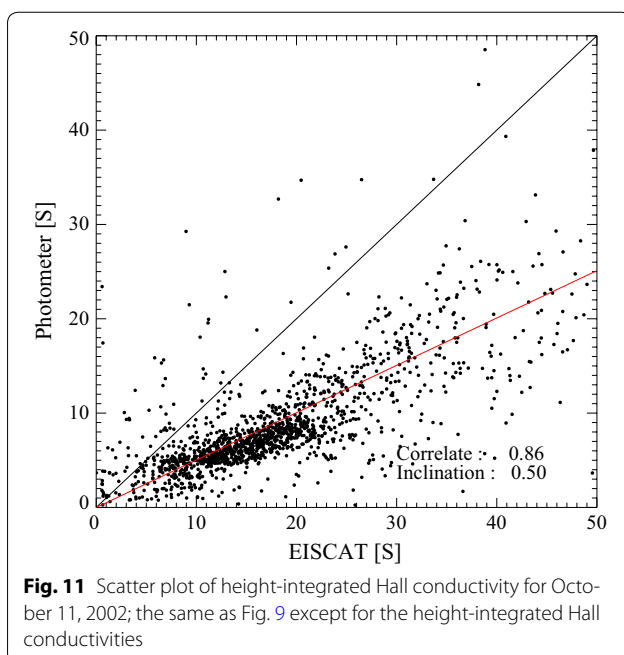
spectra obtained for a discrete aurora where the particle is accelerated have a sharper structure than that of the Maxwellian distribution (Strickland et al. 1989).

Figure 12 compares two altitude profiles of the electron density (top) observed with the EISCAT UHF radar (closed circles with thinner solid lines) and deduced from the photometer observations (red solid lines) together with sky images (bottom) taken by the digital camera. To investigate an effect of the assumed energy spectrum, two sets of altitude profiles for different times are presented. Good agreement is found for the altitude profile below  $\sim 125$  km at 2054:20 UT on October 10, 2002, when a diffuse aurora was in the view of the EISCAT and the photometer, while at 2053:00 UT on October 10, 2002, when the discrete arc was probably in the view, the electron density below  $\sim 130$  km observed with the EISCAT UHF radar is significantly larger than that deduced from the photometer measurements. This result suggests that the energy spectrum assumed as the Maxwellian distribution failed to reproduce an electron density profile in the case of the discrete arc aurora.



Based on rocket observations, Ogasawara et al. (2006) reported that most of the observed energy spectra of precipitating electrons were well expressed by kappa distributions with the thermal energy of a few hundreds of

eV, while the spectrum inside a strong arc was better fitted by the sum of a Maxwellian distribution on the lower energy side and a power law at higher energies. Lanchester et al. (1997) also reported that a combined energy distribution of the Maxwellian and Gaussian distributions can reproduce the altitude profile of the electron density for an aurora with a sharp structure well. Furthermore, Miyoshi et al. (2015) showed that electrons with a wide energy range (tens of keV and a few hundred keV) simultaneously precipitated into the ionosphere during pulsating aurora in the morning side. It is quite difficult to reproduce such high-energy precipitation flux using only the two aurora emissions with assumption of Maxwellian distribution. These previous results can (at least partly) explain the reason why the Hall conductivity derived with the photometric method was underestimated in almost the entire interval. A similar trend can be found for the Pedersen conductivity during the same intervals. These results would suggest inadequate assumption of the energy spectrum shape that would cause underestimation of the Pedersen and Hall conductivities from the photometric method.



#### Long lifetime of the emission line at 630 nm

The emission at 630.0 nm is a forbidden transition of the electronic state of oxygen atoms from  $O(^1D)$  to  $O(^3P)$  with a long lifetime ( $\sim 110$  s). Ono and Hirasawa

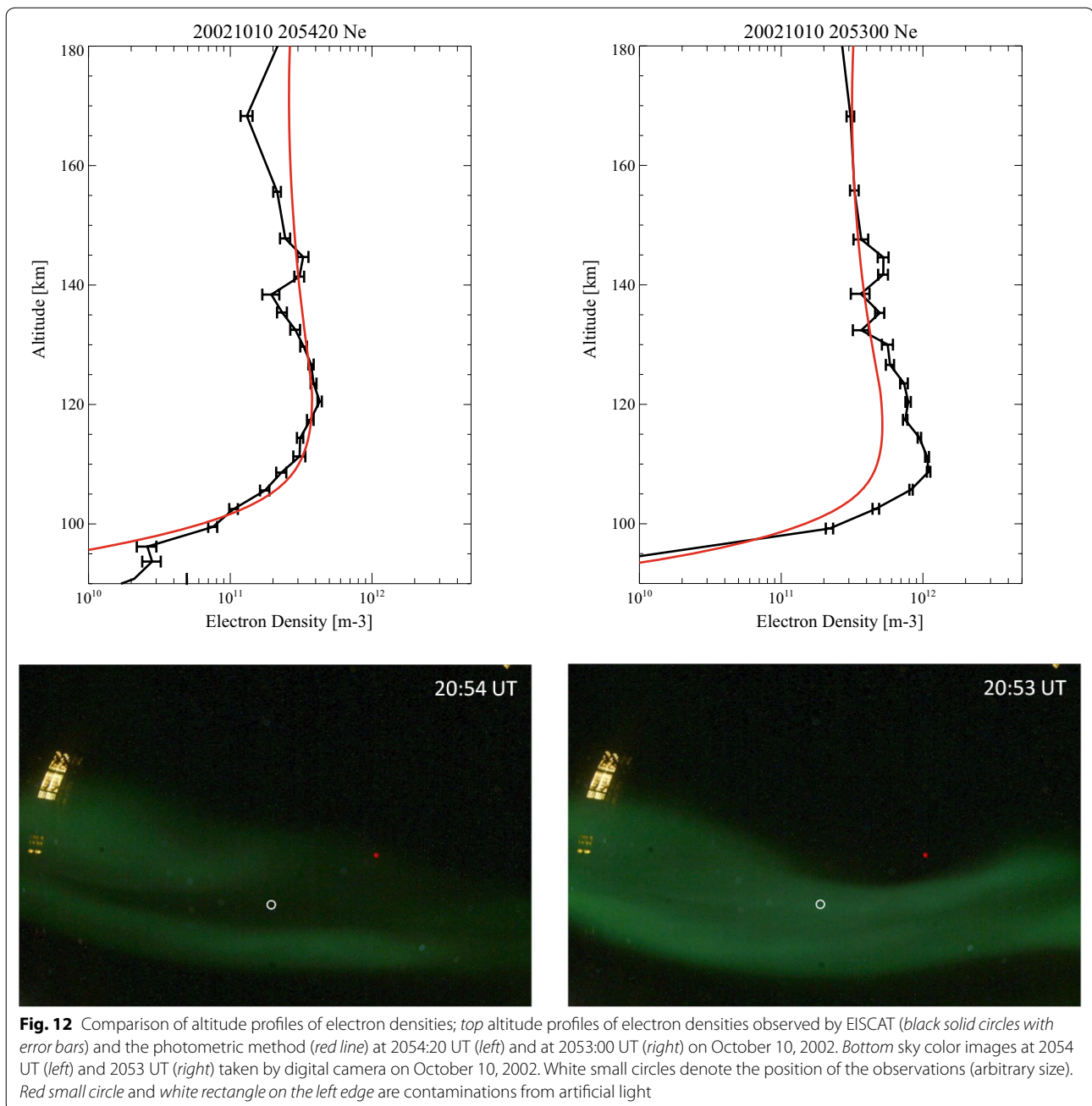


**Fig. 12** Comparison of altitude profiles of electron densities; *top* altitude profiles of electron densities observed by EISCAT (black solid circles with error bars) and the photometric method (red line) at 2054:20 UT (left) and at 2053:00 UT (right) on October 10, 2002. *Bottom* sky color images at 2054 UT (left) and 2053 UT (right) taken by digital camera on October 10, 2002. White small circles denote the position of the observations (arbitrary size). Red small circle and white rectangle on the left edge are contaminations from artificial light

(1992) reported that the emission intensity at 630.0 nm has a tendency to gradually decrease with a time constant of 35–40 s. We utilized 10-s post-integrated data in this study. Considering the emission at 630 nm lasts for approximately 40 s, it would introduce a significant contamination to the derived average energy when the amount of precipitating aurora significantly varies with time and space. In particular, the validity of the derived average energy is a strong concern when the intensity of aurora light varies quickly with time. When a discrete

arc passes through the field of view of the photometer, it would cause underestimation of the average energy of the particle precipitation.

Figure 13 illustrates temporal variations of the intensity at (a) 427.8 nm and (b) 630 nm, (c) the derived average energy, and (d) Pedersen conductivities derived by the photometer method from 23:34 UT to 23:50 UT on October 11, 2002. On the bottom panel, the Pedersen conductivities derived from the EISCAT observations are also shown by a thinner solid line for comparison.

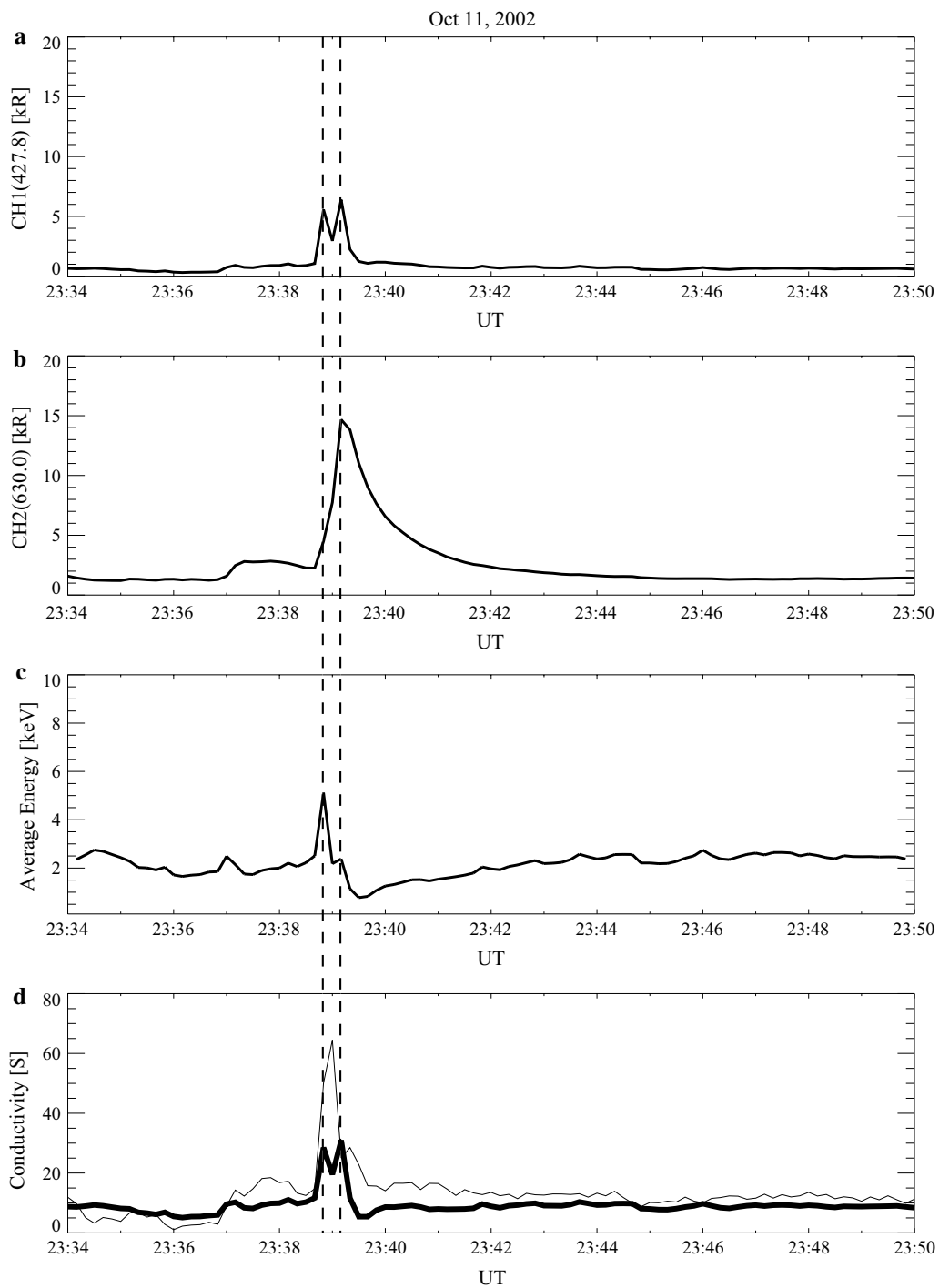


**Fig. 13** Results from 2334 to 23:50 UT on October 11, 2002; temporal variations of emission intensities at **a** 427.8 nm and **b** 630.0 nm, **c** the average energy of the precipitating electrons derived from the ratio of the two emission lines, and **d** the height-integrated Pedersen conductivity from 2334 to 23:50 UT on October 11, 2002, are shown. The temporal resolution is 10 s. On the *bottom panel*, the height-integrated Pedersen conductivity derived with the EISCAT UHF radar observation is also shown by a *thinner solid line*

Furthermore, Fig. 14 illustrates sky images taken by the digital camera at 23:38 UT (top), 23:39 UT (middle), and 23:40 UT (bottom) on October 11, 2002. At 2338:50

UT, the emission intensity at 427.8 nm sharply increased and varied quickly with time over 50 s, while the emission intensity at 630 nm increased gradually, it took 30 s



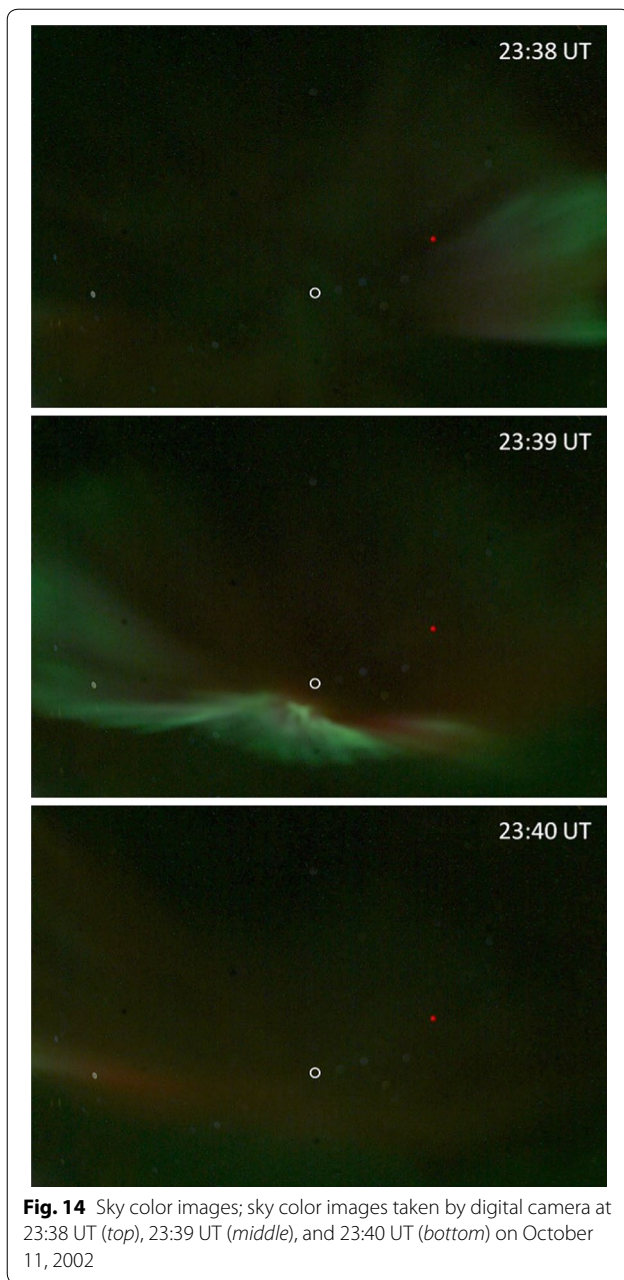


**Fig. 14** Sky color images; sky color images taken by digital camera at 23:38 UT (top), 23:39 UT (middle), and 23:40 UT (bottom) on October 11, 2002

before reaching its maximum, and higher emission intensity lasted for a few minutes. These features can be due to the difference of the time constant of the two emission lines; the emission line at 630.0 nm has a longer lifetime. Furthermore, the depletion of the average energy at 2339:10–2341:50 UT is found in Fig. 13c. For example, the underestimation of the average energy causes underestimation and overestimation of the electron density below  $\sim 140$  km and above  $\sim 160$  km, respectively. Regarding the temporal variation of the Pedersen conductivity, the sharp increase and decrease synchronize well with

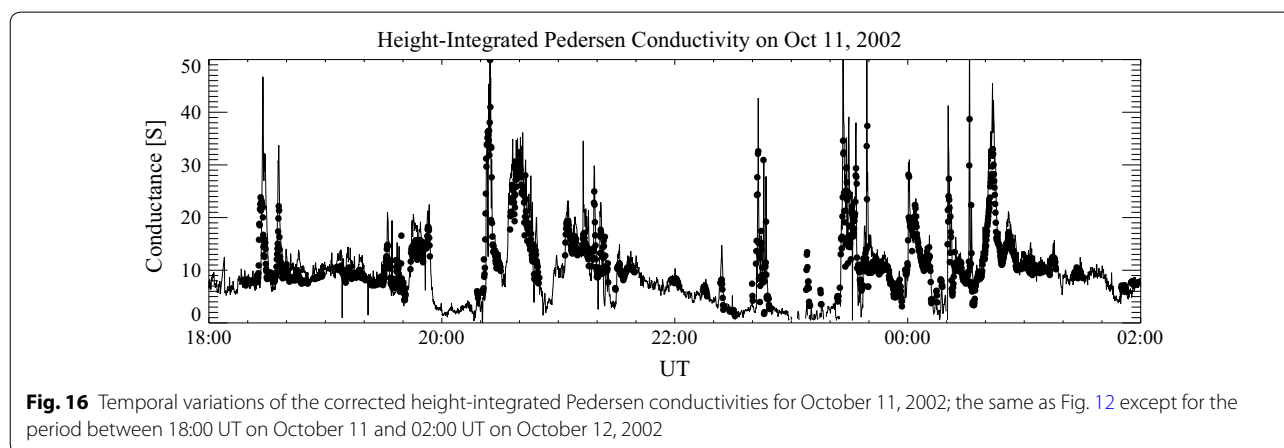
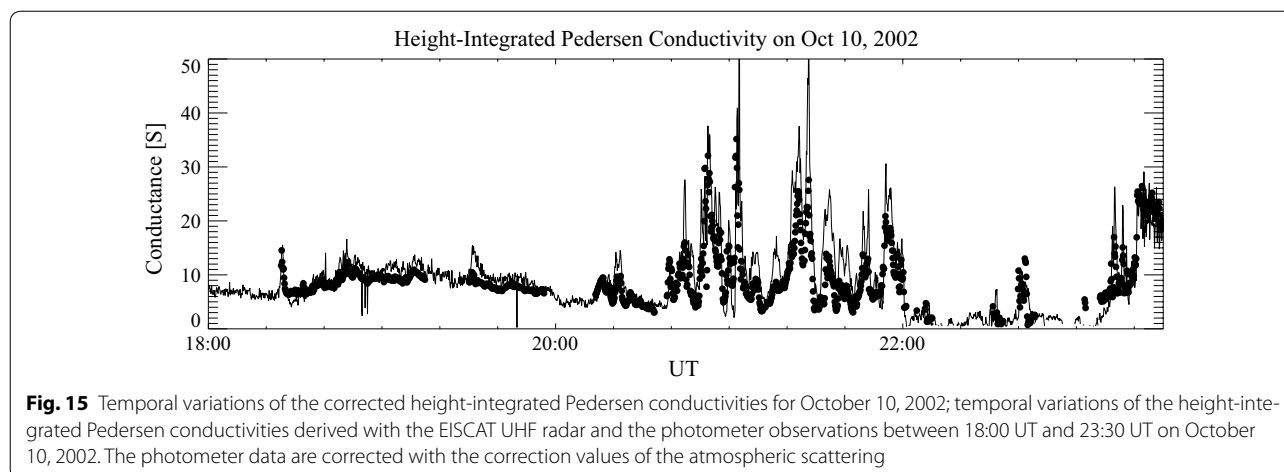
the emission intensity at 427.8 nm. A disagreement with the EISCAT radar observations as found in Fig. 13d is significant between 2338:50 and 2339:30 UT. This suggests that care is required for derivation of the Pedersen conductivity from the photometer observations for the arc-like aurora as well as the aurora with strong emission intensity at 630 nm. The underestimation of the average energy affects the Hall conductivity more seriously since the electron density below  $\sim 120$  km contributes more significantly to the Hall conductivity. Furthermore, the long lifetime of  $O(^1D)$  would cause another unavoidable contamination that is an advection effect by thermospheric wind. The advection is always a problem of phenomena with long lifetime at a point measurement. This effect also should be kept in mind when we use the method.

#### Contamination/scattering of the emission line due to the atmosphere

Atmospheric scatter influences the intensity of the photometer observations. Gattinger et al. (1991) showed the effect of increasing the Mie scattering by the model simulations. We used Table 2 of Gattinger et al. (1991) in which the correction value of the emission at 427.8 nm is 1.37 ( $=1/0.73$ ). For the emission at 630.0 nm, a linear interpolation is made of the results of Table 2 of Gattinger et al. (1991) that was the same as those of Hecht et al. (1999). Thus, the emission at 630.0 nm would be increased by 1.31. These correction values should apply, principally, for the situation when the auroral arc is just into the field of view. Here, however, we calculated the conductivities using the corrected emission intensities over the whole intervals. Figures 15 and 16 compare the height-integrated Pedersen conductivities derived from the EISCAT UHF radar (solid line) and from the corrected emission intensities (filled circles) on October 10 and 11, 2002, respectively. These figures show better (and excellent) agreements between the two different methods and indicate that the corrections of atmospheric scattering are necessary. However, even using these correction values, the Hall conductivities derived by the photometric observations are still smaller than those derived by the EISCAT radar.

#### Contributions from proton precipitations

In this analysis, energetic electrons have been taken into account as the only source of ionization. Several studies (Basu et al. 1987; Senior 1991; Galand and Richmond 2001) have, however, shown that energetic protons play a major role in producing ionospheric electrons and conductance at given locations and times, particularly in the cusp and at the equatorward boundary of the auroral oval before geomagnetic midnight. Senior (1991) compared



the height-integrated conductivities derived from EISCAT data with a statistical model of conductance obtained from precipitating electron characteristics measured by the DMSP satellites. She found that the EISCAT-derived conductance agreed well with that from the DMSP model in the morning sector but was systematically larger than that of the model in the evening sector. She suggested that this difference is due to the *E* region electron production from energetic proton precipitations, which occurs preferentially in the evening sector. This idea could partly explain the facts shown here that demonstrate that the Pedersen and Hall conductivities seem to be underestimated by the photometric method. We could not distinguish the auroral emissions due to electrons and/or protons, because observations of proton auroral emissions such as  $H_{\alpha}$  or  $H_{\beta}$  were not conducted in October 2002. In order to distinguish the effect of the energetic protons as well as to derive conductivities more accurately, observations of proton auroras should be carried out together, and the contributions of protons to the ionospheric conductivities should be taken into account properly.

#### Collision cross section between atom oxygen and electron

To calculate the auroral emission ratio needed for deducing the characteristic electron energy, we have applied the model presented in Ono (1993), where for the population of  $O(^1D)$ , three production processes and two loss processes were taken into account. A dominant mechanism of the  $O(^1D)$  state in his model is a direct electron impact (cf. Solomon et al. 1988). Ono (1993) used the theoretical electron impact excitation cross section of the  $O(^1D)$  state from Banks et al. (1974) that was originally presented by Green and Stolarski (1972). Johnson et al. (2005) reviewed the comprehensive analyses of experimental and theoretical cross-sectional values, and then, they showed that there are significant differences between both values of theoretical and experimental cross sections of  $O(^1D)$  state excitation (see Fig. 3 of Johnson et al. 2005). Doering (1992) presented that although his experimental values were in excellent agreement with theoretic values at incident energies greater than 9 eV, at lower incident energies the experimental values had a sharp peak nearby 6 eV, approximately by

factor 2 larger than theoretic values by Lan et al. (1972). It seems like that the cross-sectional values used in Ono (1993) would be lower than the experimental values in factor 2 or so. This would be another cause for discrepancy between photometric and EISCAT values; the Hall conductivities would be underestimated.

**Composition of the atmosphere predicted by NRLMSISE-00**

The neutral atmosphere density would contribute to the discrepancy in the conductivities calculated by the two methods. The models of the auroral red (630.0 nm) line predict strong dependence of its intensity on the ratio of the thermospheric atomic oxygen (O) to the molecular nitrogen (N<sub>2</sub>) concentration. Hecht et al. (2012) compared NRLMSISE-00 predictions over the year 2002–2006 for column O/N<sub>2</sub> with TIMED/GUVI daytime observations as well as photometer (nighttime) observations made at two high latitude stations at Poker Flat (65.1°N, 212.5°E) and Fort Yukon (66.6°N, 214.7°E). Hecht et al. (2012) showed that while the nighttime observations

showed considerable agreement with NRLMSISE-00 predictions, they were much more variable (+/- about 35%) than the predictions, suggesting that there are significant local effects in the auroral zone that are not captured by the model. This is also another cause (but we believe the usage of NRLMSISE-00 is the best option).

**Dependencies of the conductivities on the cross section and the atomic oxygen density**

As mentioned above, the cross section as well as the atomic oxygen density affects derived conductivities by the photometric method. To investigate those dependencies, we have calculated conductivities by using double and half those values used and have compared them with those derived using the normal values. Results are presented in Figs. 17 and 18 for the nights of October 10 and 11, respectively. These figures show temporal variations of ratios of height-integrated conductivities: Red and blue circles denote ratios of values when the corresponding values (i.e., cross section or atom oxygen

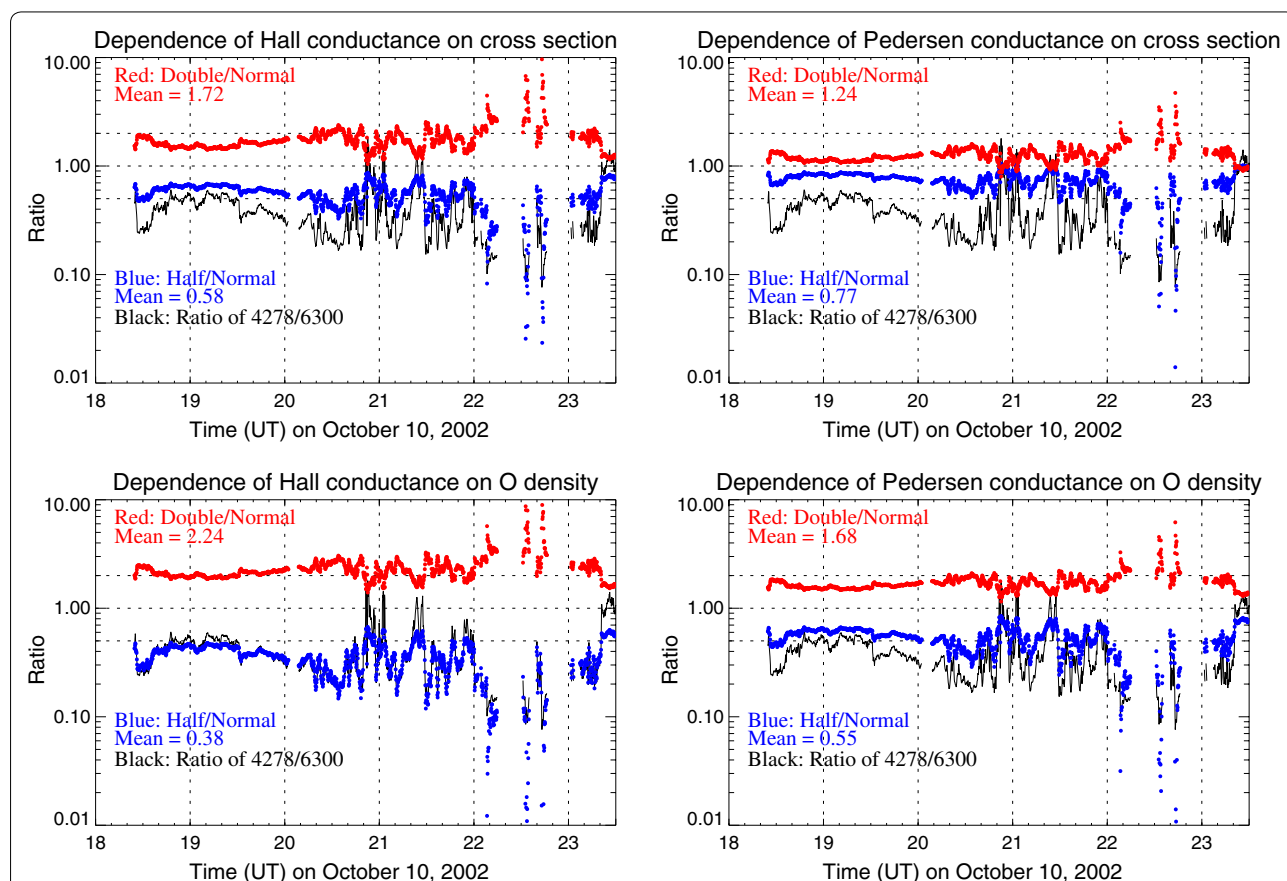
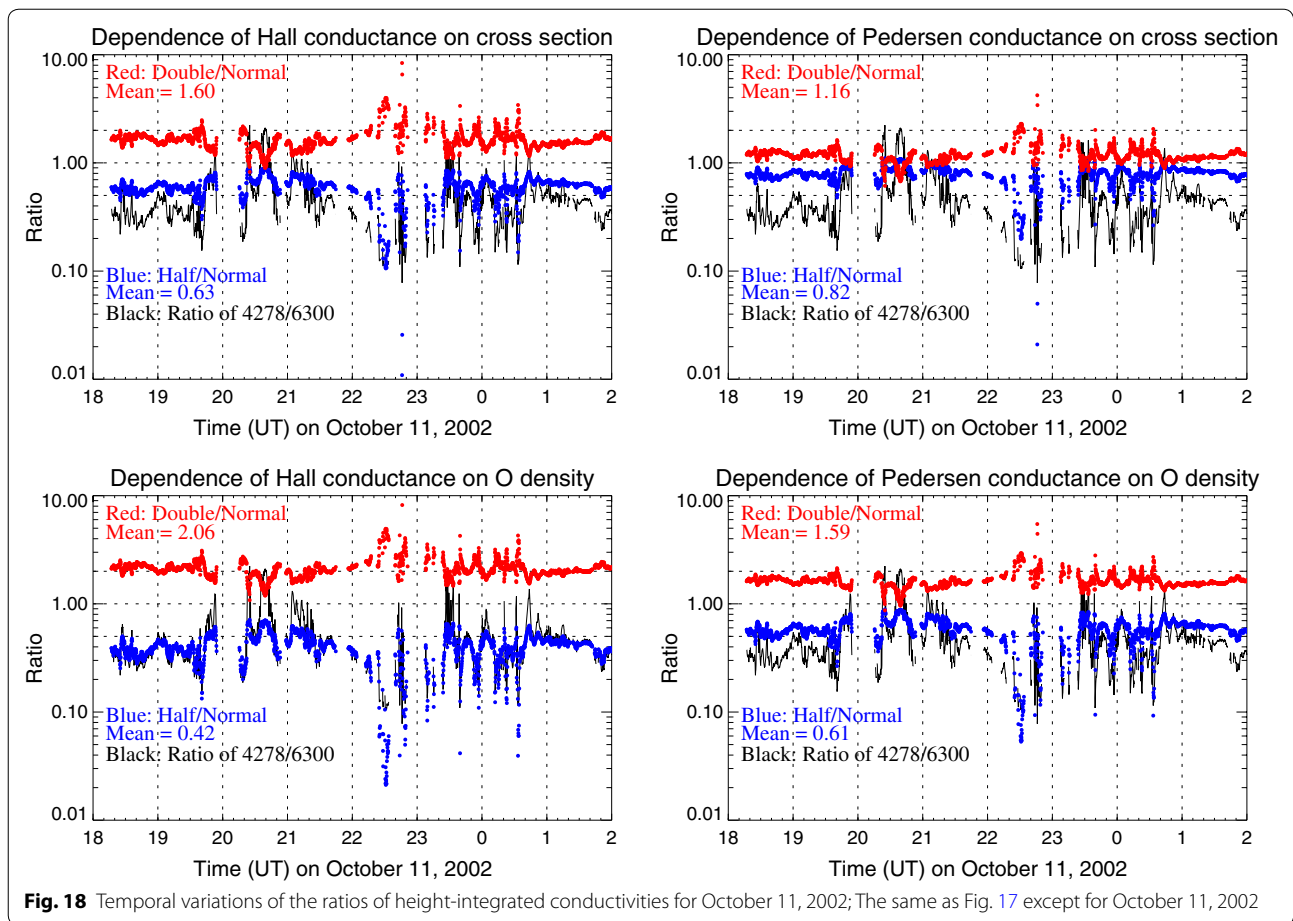


**Fig. 17** Temporal variations of the ratios of height-integrated conductivities for October 10, 2002; temporal variations of ratios of height-integrated Hall (left) and Pedersen (right) conductivities as well as intensity ratios of 427.8 to 630 nm for October 10, 2002. Upper panels: Red and blue circles denote the ratios of values when the cross-sectional values are doubled or halved to the normal values, respectively. Lower panels: same to the upper panels but for atomic oxygen density



density) are doubled and halved to the normal values, respectively. The upper and lower panels present dependencies of the cross section and the atomic oxygen density, respectively. The intensity ratios of 427.8 to 630 nm ( $I_{4278}/I_{6300}$ ) are also presented. The averaged conductivity ratios are summarized in Table 1. First of all, we easily realize both the cross section and the atom oxygen density could introduce large ambiguities to the derived conductivities by the photometric method. Hall conductivity is more seriously affected by those values than Pedersen

conductivity. Concerning the atomic oxygen density, if we double (half) it, Hall conductivity becomes more than double (less than half), indicating that the realistic estimate of the atomic oxygen density is essential. The cross section also introduces significant differences; when we double it, Hall and Pedersen conductivities are increased by 60–70% and about 20%, respectively. This would suggest if we use the double value of the cross section for the derivation of conductivities, the agreement between derived conductivities by photometer and

**Table 1** Dependences of the Hall and Pedersen height-integrated conductivities on the cross section and oxygen atom density

Ratio	Cross section				Oxygen atom density			
	Double/normal		Half/normal		Double/normal		Half/normal	
	Hall	Ped	Hall	Ped	Hall	Ped	Hall	Ped
October 10	1.60	1.16	0.63	0.82	2.06	1.59	0.42	0.61
October 11	1.72	1.24	0.58	0.77	2.24	1.68	0.38	0.55

Ped Pedersen

EISCAT will be better. When the intensity ratio ( $I_{427.8}/I_{630.0}$ ) becomes higher (corresponding to time interval of higher energy precipitation), the dependence becomes lower (but nonzero). Furthermore, when the intensity of 427.8 nm becomes darker (i.e., the intensity ratio become lower, e.g., between 22:10 and 23:20 UT on October 10), the dependence of conductivity is increased significantly, suggesting that the photometric method involves significantly larger ambiguities for such a case.

## Conclusion

Simultaneous observations were conducted by using a multi-wave photometer and the EISCAT UHF radar at Tromsø for the two nights of October 10 and 11, 2002. By using these data sets, we compared electron density profiles as well as Pedersen and Hall height-integrated conductivities in order to evaluate the photometric method using two emission lines at 427.8 and 630.0 nm. In general, good agreement was found between height-integrated conductivities derived by the EISCAT UHF radar and photometer in terms of temporal variations, indicating that the optical method using the two emission intensities of 427.8 and 630.0 nm basically has the ability to derive conductivities for (diffuse) auroras. In cases of auroral arcs coming into the field of view of the photometer, the difference between the two methods is significant. We have discussed possible causes of the differences: incorrect assumption of the shape of the energy spectrum of the precipitating particles, the long lifetime (~110 s) of the emission line at 630 nm, contaminations/scattering of the emission line by the atmosphere, energetic proton precipitations, collision cross section between atom oxygen and electron, and composition of the atmosphere predicted by NRLMSISE-00. In the cases of discrete arc auroras, the energy spectrum of the precipitating particles can no longer be assumed to be the Maxwellian distribution. Also owing to the long lifetime of the 630 nm line, the derived average energy of particle precipitations can be overestimated and underestimated. Underestimation of the average energy causes electron density to be overestimated above ~160 km and underestimated below ~140 km. Therefore, care is necessary to analyze photometric observational data in cases of a discrete arc aurora, and it is of vital importance that simultaneous monitoring of auroras be carried out together with photometric observations. Furthermore, usage of incorrect collision cross section between atom oxygen and electron as well as composition change during the high auroral activity should also increase ambiguities for derivation of conductivities. Finally, we conclude that, even though photometer measurements are weakened by these limitations, the photometric method using the two wavelengths (427.8 and 630.0 nm)

is very valuable for deriving ionospheric conductances (at least for the Pedersen conductance) due to its easy installation/operation.

## Abbreviations

AIRS: auroral ionospheric remote sensor; CP1: Common Program One; EISCAT: European Incoherent Scatter; FAC: field-aligned current; IGRF: International Geomagnetic Reference Field; IRI: International Reference Ionosphere; IS: incoherent scatter; KST: Kiruna–Sodankylä–Tromsø; NIPR: National Institute of Polar Research.

## Authors' contributions

KA developed/operated the photometer system, analyzed data, and provided scientific results. SN analyzed data and organized the manuscript. YO contributed to the operation of the photometer and analysis of data, and science. AB contributed to the operation and science. CH contributed to the operation and science. RF designed the science plan first and contributed to science. All authors read and approved the final manuscript.

## Author details

<sup>1</sup>Institute for Space-Earth Environmental Research, Nagoya University, Furo-cho, Chikusa-ku, Nagoya, Japan. <sup>2</sup>National Institute of Polar Research, 10-3, Midori-cho, Tachikawa-shi, Tokyo 190-8518, Japan. <sup>3</sup>Faculty of Science, The Arctic University of Norway, 9037 Tromsø, Norway. <sup>4</sup>Tromsø Geophysical Observatory, The Arctic University of Norway, 9037 Tromsø, Norway.

## Acknowledgements

We are indebted to the director and staff of EISCAT for operating the facility and supplying the data. EISCAT is an International Association supported by China (CRIRP), Finland (SA), Japan (ISEE and NIPR), Norway (NFR), Sweden (VR), and the UK (NERC). The four-wavelength photometer was calibrated using the optical facility at the National Institute of Polar Research, Japan. This study was partly supported by Grants-in-Aid for Scientific Research (15H05747 and 17H02968) of Japan Society for the Promotion of Science (JSPS) and by JSPS Program for Advancing Strategic International Networks to Accelerate the Circulation of Talented Researchers under Grant G2602.

## Competing interests

The authors declare that they have no competing interests.

## Publisher's Note

Springer Nature remains neutral with regard to jurisdictional claims in published maps and institutional affiliations.

Received: 30 August 2016 Accepted: 27 June 2017

Published online: 03 July 2017

## References

- Banks PM, Nagy AF (1970) Concerning the influence of elastic scattering upon photoelectron transport and escape. *J Geophys Res* 75:1902–1910
- Banks PM, Chappell CR, Nagy AF (1974) A new model for the interaction of auroral electrons with the atmosphere: spectral degradation, backscatter, optical emission, and ionization. *J Geophys Res* 79:1459–1470
- Basu B, Jasperse JR, Robinson RM, Vondrak RR, Evans DS (1987) Linear transport theory of auroral proton precipitation—a comparison with observations. *J Geophys Res* 92:5920–5932
- Blitz D (2001) International Reference Ionosphere 2000. *Radio Sci* 36:261–276
- Brekke A, Hall C (1988) Auroral ionospheric quiet summer time conductances. *Ann Geophys* 6:361–375
- Brekke A, Doupnik J, Banks PM (1974) Incoherent scatter measurements of *E* region conductivities and currents in the auroral zone. *J Geophys Res* 79:3773–3790
- Collis PN (1995) EISCAT data base for ionospheric modelling: F-region and topside ionosphere. *Adv Space Res* 16:37–46
- Coumans V, Gerard J-C, Hubert B, Meurant M, Mende SB (2004) Global auroral conductance distribution due to electron and proton precipitation from IMAGE-FUV observations. *Ann Geophys* 22:1595–1611



- Doering JP (1992) Absolute differential and integral electron excitation cross sections for atomic oxygen: 9. Improved cross section for the  $^3P \rightarrow ^1D$  transition from 4.0 to 30 eV. *J Geophys Res* 97(A12):19531–19534
- Folkstad K, Hagfors T, Westerlund S (1983) EISCAT—an updated description of technical characteristics and operational capabilities. *Radio Sci* 18:867–879
- Fontaine D, Peymirat C (1996) Large-scale distributions of ionospheric horizontal and field-aligned currents inferred from EISCAT. *Ann Geophys* 14:1284–1296
- Galand M, Richmond AD (2001) Ionospheric electrical conductances produced by auroral proton precipitation. *J Geophys Res* 106:117–126
- Gattinger RL, Vallance Jones A, Hecht JH, Strickland DJ, Kelley J (1991) Comparison of ground-based optical observations of  $N_2$  second positive to  $N_2^+$  first negative emission ratios with electron precipitation energies inferred from the Sondre Stromfjord radar. *J Geophys Res* 96:11341–11351
- Green AES, Stolarski RS (1972) Analytic models of electron impact excitation cross sections. *J Atmos Terr Phys* 34:1703–1717
- Greenwald RA, Baker KB, Dudeney JR, Pinnock M, Jones TB, Thomas EC, Villain JP, Cerisier JC, Senior C, Hanuise C (1995) Darn/Superdarn: a global view of the dynamics of high-latitude convection. *Space Sci Rev* 71:761–796
- Hall CM, Hansen TL (2003) 20th century operation of the Tromsø Ionosonde. *Adv Polar Upper Atmos Res* 17:155–166
- Hecht JH, Christensen AB, Strickland DJ, Majeed T, Gattinger RL, Vallance Jones A (1999) A comparison between auroral particle characteristics and atmospheric composition inferred from analyzing optical emission measurements alone and in combination with incoherent scatter radar measurements. *J Geophys Res* 104:33–44
- Hecht JH, Mulligan T, Correia JT, Clemmons JH, Strickland DJ, Walterscheid RL, Conde MG (2012) A multiyear (2002–2006) climatology of  $O/N_2$  in the lower thermosphere from TIMED GUVI and ground-based photometer observations. *J Geophys Res*. doi:10.1029/2011JA017146
- Heinselman CJ (2000) Auroral effects on the gas phase chemistry of meteoric sodium. *J Geophys Res* 105:12181–12192
- Johnson PV, McConkey JW, Tayal SS, Kanik I (2005) Collisions of electrons with atomic oxygen: current status. *Can J Phys* 83:589–616
- Kurihara J (2004) Energetics and structure of the lower thermosphere observed by sounding rocket experiment. Dissertation, Tokyo University
- Lan Vo Ky, Feautrier N, LeDourneuf M, Van Regemorter H (1972) Cross sections calculations for electron-oxygen scattering using the polarized orbital close coupling theory. *J Phys B At Mol Phys* 5:1506–1516
- Lanchester BS, Rees MH, Lummerzheim D, Otto A, Frey HU, Kaila KU (1997) Large fluxes of auroral electrons in filaments of 100 m width. *J Geophys Res* 102:9741–9748
- Lanchester BS, Ashrafi M, Ivchenko N (2009) Simultaneous imaging of aurora on small scale in OI (777.4 nm) and N21P to estimate energy and flux of precipitation. *Ann Geophys* 27:2881–2891
- Mende SB, Vondrak RR, Eather RH, Rees MH, Robinson RM (1984) Optical mapping of ionospheric conductance. *J Geophys Res* 89:1755–1763
- Miyoshi Y, Oyama S, Saito S, Kurita S, Fujiwara H, Kataoka R, Ebihara Y, Kletzing C, Reeves G, Santolik O, Ciliverd M, Rodger CJ, Turunen E, Tsuchiya F (2015) Energetic electron precipitation associated with pulsating aurora: EISCAT and Van Allen Probe observations. *J Geophys Res* 120:2754–2766. doi:10.1002/2014JA020690
- Nagy AF, Banks PM (1970) Photoelectron fluxes in the ionosphere. *J Geophys Res* 75:6260–6270
- Niciejewski RJ, Meriwether JW Jr, Valliance Jones A, Gattinger RL, Valladares CE, Wickwar VB, Kelly J (1989) Ground-based observations of  $O_2^+$  1 N band enhancements relative to  $N_2^+$  1 N band emission. *Planet Space Sci* 37:131–143
- Ogasawara K, Asamura K, Takashima T, Saito Y, Mukai T (2006) Rocket observation of energetic electrons in the low-altitude auroral ionosphere during the DELTA campaign. *Earth Planets Space* 58:1155–1163. doi:10.1186/BF03352005
- Olsen N, Sabaka TJ, Tøffner-Calausen L (2000) Determination of the IGRF 2000 model. *Earth Planets Space* 52:1175–1182. doi:10.1186/BF03352349
- Ono T (1993) Derivation of energy parameters of precipitating auroral electrons by using the intensity ratios of auroral emissions. *J Geomag Geoelectr* 45:455–472
- Ono T, Hirasawa T (1992) An apparent lifetime of auroral 630.0 nm (OI) emissions. *J Geomag Geoelectr* 44:91–108
- Picone JM, Hedin AE, Drob DP, Aikin AC (2002) NRLMSISE-00 empirical model of the atmosphere: statistical comparisons and scientific issues. *J Geophys Res*. doi:10.1029/2002JA009430
- Rees MH (1963) Auroral ionization and excitation by incident energetic electrons. *Planet Space Sci* 11:1209–1218
- Rees MH, Luckey D (1974) Auroral electron energy derived from ratio of spectroscopic emissions. I—model computations. *J Geophys Res* 79:5181–5186
- Rishbeth H, van Eyken AP (1993) EISCAT—early history and the first ten years of operation. *J Atmos Terr Phys* 55:525–542
- Robinson RM, Vondrak RR (1994) Validation of techniques for space based remote sensing of auroral precipitation and its ionospheric effects. *Space Sci Rev* 69:331–407
- Robinson RM, Vondrak RR, Craven JD, Frank LA, Miller K (1989) A comparison of ionospheric conductances and auroral luminosities observed simultaneously with the Chatanika radar and the DE 1 auroral imagers. *J Geophys Res* 94:5382–5396
- Robinson R, Dabbs T, Vickrey J, Eastes R, del Greco F, Huffman R, Meng C, Daniell R, Strickland D, Vondrak R (1992) Coordinated measurements made by Sondrestrom radar and Polar Bear Ultraviolet Imager. *J Geophys Res* 97:2863–2871
- Schunk RW, Nagy AF (1978) Electron temperatures in the F region of the ionosphere—theory and observations. *Rev Geophys Space Phys* 16:355–399
- Schunk RW, Walker JCG (1973) Theoretical ion densities in the lower ionosphere. *Planet Space Sci* 21:1875–1896
- Semeter J, Kamalabadi F (2005) Determination of primary electron spectra from incoherent scatter radar measurements of the auroral E region. *Radio Sci*. doi:10.1029/2004RS003042
- Senior C (1991) Solar and particle contributions to auroral height-integrated conductivities from EISCAT data—a statistical study. *Ann Geophys* 9:449–460
- Solomon SC, Hays PB, Abreu VJ (1988) The auroral 6300 Å emission: observations and modeling. *J Geophys Res* 93:9867–9882
- Strickland DJ, Meier RR, Hecht JH, Christensen AB (1989) Deducing composition and incident electron spectra from ground-based auroral optical measurements: theory and model results. *J Geophys Res* 94:13527–13539
- Strickland DJ, Daniell RE Jr, Jasperse JR, Basu R (1993) Transport-theoretic model for the electron-proton-hydrogen atom aurora, 2. Model results. *J Geophys Res* 98:21533–21548
- Sugino M, Fujii R, Nozawa S, Nagatsuma SCT, Buchert HJ, Opgenoorth JW, Gjerloev, Kosch MJ (2002a) Field-aligned currents and ionospheric parameters deduced from EISCAT radar measurements in the post-midnight sector. *Ann Geophys* 20:1335–1348
- Sugino M, Fujii R, Nozawa S, Buchert SC, Opgenoorth HJ, Brekke A (2002b) Relative contribution of ionospheric conductivity and electric field to ionospheric current. *J Geophys Res*. doi:10.1029/2001JA007545
- Vondrak RR, Sears RD (1978) Comparison of incoherent scatter radar and photometric measurements of the energy distribution of auroral electrons. *J Geophys Res* 83:1665–1667
- Vondrak RR, Murphree JS, Anger CD (1985) Remote sensing of high-latitude ionization with ISIS2 auroral scanning photometer. *Radio Sci* 20:439–446

Submit your manuscript to a SpringerOpen® journal and benefit from:

- Convenient online submission
- Rigorous peer review
- Open access: articles freely available online
- High visibility within the field
- Retaining the copyright to your article

Submit your next manuscript at ► [springeropen.com](http://springeropen.com)